Hindawi
Advances in Civil Engineering
Volume 2018, Article ID 9178140, 7 pages
https://doi.org/10.1155/2018/9178140

Research Article

Influence of Structural Plane Microscopic Parameters on Direct Shear Strength

Yanhui Cheng[1,2] **Weijun Yang,**[1] **and Dongliang He**[1,2]

[1]*School of Civil Engineering, Changsha University of Science and Technology, Changsha 410114, China*
[2]*School of Civil Engineering, Hunan University of City, Yiyang, Hunan 413000, China*

Correspondence should be addressed to Yanhui Cheng; chengyanhuihn@126.com

Received 28 March 2018; Revised 3 May 2018; Accepted 11 June 2018; Published 2 July 2018

Academic Editor: Hang Lin

Structural plane is a key factor in controlling the stability of rock mass engineering. To study the influence of structural plane microscopic parameters on direct shear strength, this paper established the direct shear mechanical model of the structural plane by using the discrete element code PFC2D. From the mesoscopic perspective, the research on the direct shear test for structural plane has been conducted. The bonding strength and friction coefficient of the structural plane are investigated, and the effect of mesoscopic parameters on the shear mechanical behavior of the structural plane has been analyzed. The results show that the internal friction angle φ of the structural plane decreases with the increase of particle contact stiffness ratio. However, the change range of cohesion is small. The internal friction angle decreases first and then increases with the increase of parallel bond stiffness ratio. The influence of particle contact modulus EC on cohesion c is relatively small. The internal friction angle obtained by the direct shear test is larger than that obtained by the triaxial compression test. Parallel bond elastic modulus has a stronger impact on friction angle φ than that on cohesion c. Under the same normal stress conditions, the shear strength of the specimens increases with particle size. The shear strength of the specimen gradually decreases with the increase of the particle size ratio.

1. Introduction

The large-scale existence of structural plane has severely damaged the continuity and integrity of rock mass, thereby exerting a profound influence on the strength of the rock mass. Structural plane is a key factor in controlling the stability of rock mass engineering [1–5]. The destruction and damage of jointed rock mass is mainly along the structural plane. Thus, studies on the shear strength, failure mode, and shear damage of a structural plane are significant. Many scholars have conducted relevant research [6–12]. Yang et al. [13] study the relationship between the 3D morphological characteristics and the peak shear strength through several tilt tests. Fardin et al. [14] carried out investigations to understand the effect of scale on the surface roughness of rock joints. Park and Song [15] have numerically simulated rock joints and performed an extensive series of the direct shear tests using the code PFC3D. PFC3D represents that the interaction of circular particles by the distinct element method (DEM) can simulate joint movement. Achieving the specified JRC value for real rock samples and considering the homogeneity of rocks are difficult because the shear test for the same roughness cannot be investigated under different conditions of laboratory tests [16–18]. In recent years, the application of discrete element numerical methods in geotechnical engineering has become extensive, and scholars have used this method to investigate the mechanical properties of joints [19–25]. Farahmand et al. [26] used a synthetic rock mass (SRM), model coupling discrete fracture networks (DFNs), and a discrete element grain-based model (DEM) to characterize the mechanical properties of moderately jointed rock masses under confined and unconfined conditions. Shang et al. [27] present a numerical investigation of the effects of boundary conditions on the failure mechanism of incipient rock discontinuities in direct shear. In this paper, the direct shear mechanical model of the structural plane is established by using the discrete element code PFC2D. From the mesoscopic perspective, the research on the direct shear test for structural plane has been conducted. The bonding strength and friction coefficient of the

Table 1: Shear strength parameter values of different particle contact stiffness ratio.

Particle contact stiffness ratio	Friction angle (°)	Cohesion (MPa)
0.5	21.16	8.75
1	24.28	8.94
1.45	20.30	9.29
2	24.56	8.73
3	22.73	8.43
4	20.41	8.52
5	19.34	8.49
6	18.62	8.52
7	17.80	8.48
8	18.52	8.25
9	19.49	8.19
10	15.70	8.29

structural plane are investigated, and the effect of mesoscopic parameters on the shear mechanical behavior of the structural plane has been analyzed.

2. Modeling

Numerical simulation of the shear strength test is divided into two categories, namely, nonlimit and restrictive shear strength tests. The nonlimit shear strength test only has shear stress on the shear surface without the existence of normal stress. The restricted shear strength test has normal stress in addition to the shear stress on the shear plane [28–31]. In this paper, the restrictive shear strength test is adopted to apply a specific normal stress on the sample, and the normal stress is set as 2.5, 5.0, 7.5, 10.0, 12.5, and 15 MPa. The size of the direct shear test is 100 mm × 100 mm, and the speed boundary condition is applied to the upper part of the model. Results show that the internal friction angle $\varphi = 20.30^{\circ}$ and cohesion $c = 9.29$ MPa.

3. Results and Analysis

3.1. Particle Contact Stiffness Ratio. The impact of particle contact stiffness ratio k_n/k_s on shear strength is shown in Table 1. The internal friction angle φ of the structural plane decreases with the increase of particle contact stiffness ratio k_n/k_s. However, the change range of cohesion is small, indicating that particle contact stiffness ratio k_n/k_s has less effect on the cohesion.

The effect of particle contact stiffness ratio on the internal friction angle is shown in Figure 1. The normal stiffness of particles increased gradually with the particle contact stiffness ratio of k_n/k_s. In the conventional triaxial compression simulation test, shear failure is the specimen failure mode, and the internal friction angle in the shear strength parameter is approximately the same as that obtained in the direct shear simulation test. However, in the direct shear simulation experiment, the particle contact stiffness ratio of $k_n/k_s = 1.45$ and $k_n/k_s = 0.5$, and the size differences between internal friction angle is extremely small, indicating if the normal stiffness is close to the tangential stiffness, then the friction angle will decrease. In the

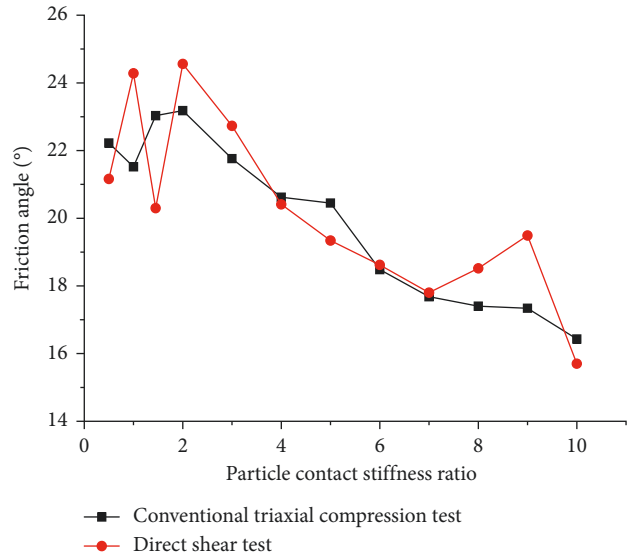

Figure 1: Influence of particle contact stiffness on friction angle.

direct shear test, when the particle contact stiffness ratio increases gradually, the internal friction angle of the structure increases gradually. When the particle contact stiffness ratio of $k_n/k_s = 2.0$, the internal friction angle reaches the peak of the specimens, which is $\varphi = 24.56^{\circ}$. For particle contact stiffness ratio $k_n/k_s = 1.0$, the internal friction angle is also relatively large at $\varphi = 24.28^{\circ}$. The internal friction angle of the specimen can be increased when the contact between particles is equal to the tangential stiffness. If the normal stiffness of the particle is greater than the tangential stiffness, then the difference between the normal and tangential stiffness is less, and the internal friction angle is less than the internal friction angle when the particle method is equal to the tangential stiffness. When the normal stiffness is twice the tangential stiffness, the internal friction angle is maximized. Particle contact stiffness ratio k_n/k_s increases to a certain value. The particles during normal stiffness are larger than those during tangential stiffness. A small internal friction angle can enhance shear strength. However, the general trend means that the internal friction angle of the specimens decreases with the increase of the particle contact stiffness ratio. The influence of particle contact stiffness ratio on cohesion is analyzed, as shown in Figure 2. The cohesion c of the specimen is less than that of the conventional triaxial compression simulation test under the same k_n/k_s. Under the two test conditions, the cohesion of the specimen has the same change trend as that of k_n/k_s, and the influence of k_n/k_s on adhesion c is relatively small.

3.2. Parallel Bond Stiffness Ratio. Parallel bond stiffness ratio is a specific parameter in the simulation of parallel bonding model, which represents the ratio of the normal stiffness to the tangential stiffness between two particles. The shear strength parameter values of different parallel bond stiffness ratios are recorded, as shown in Table 2. The internal friction angle fluctuates with the increase of parallel bond stiffness ratio $\overline{k}_n/\overline{k}_s$. When the particle parallel bond stiffness ratio is

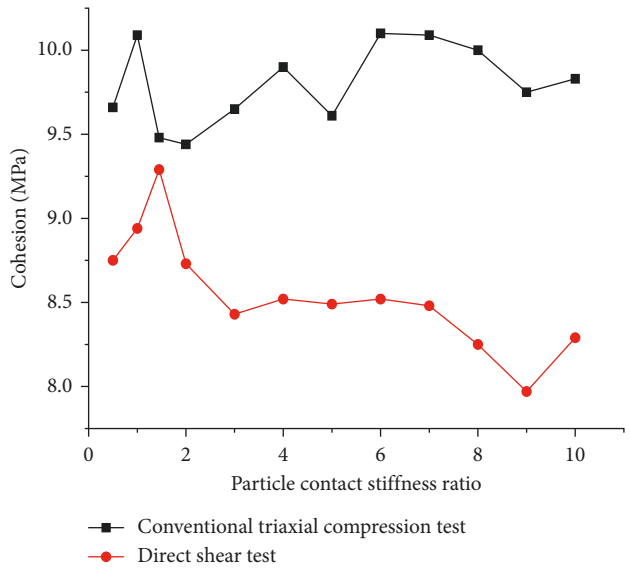

Figure 2: Influence of particle contact stiffness on cohesion.

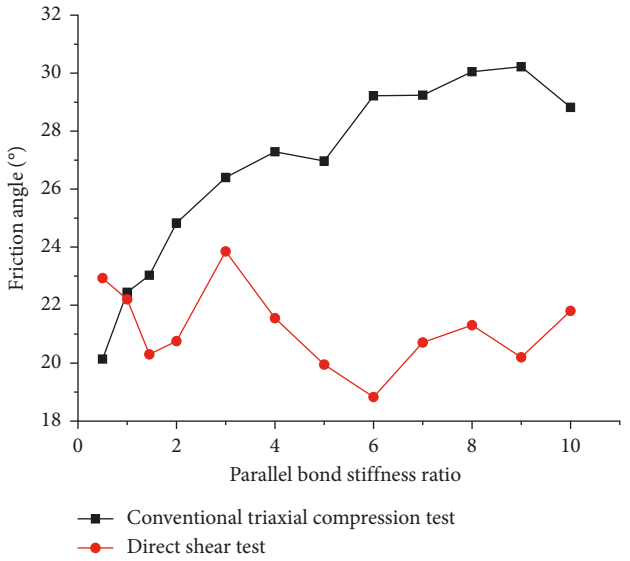

Figure 3: Influence of parallel bond stiffness on friction angle.

Table 2: Shear strength parameter values of different parallel bond stiffness ratios.

Parallel bond stiffness ratio	Friction angle (°)	Cohesion (MPa)
0.5	22.93	8.35
1	22.20	8.79
1.45	20.30	9.29
2	20.76	9.14
3	23.85	8.79
4	21.55	8.58
5	19.95	8.76
6	18.83	8.48
7	20.71	8.05
8	21.31	7.67
9	20.20	7.63
10	21.80	7.25

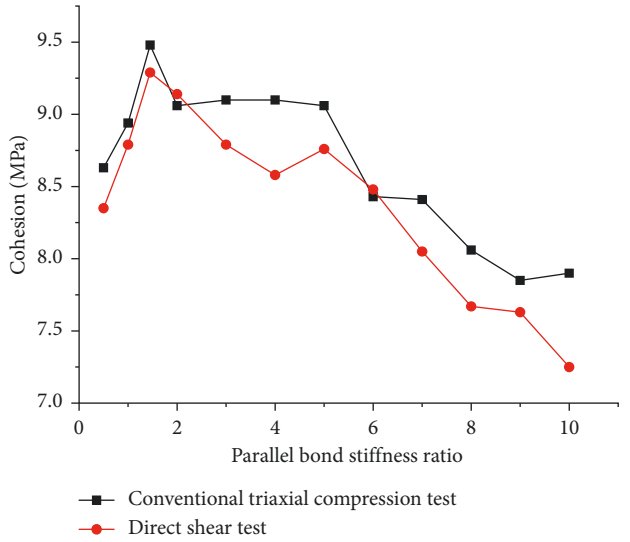

Figure 4: Influence of parallel bond stiffness on cohesion.

$\overline{k}_n/\overline{k}_s = 2$, the result of the internal friction angle is less than $\overline{k}_n/\overline{k}_s = 0.5$ because the model is a parallel bond model, which is in accordance with the shear failure model. Moreover, the particle cementing material between normal stiffness is large. The internal friction angle decreases first and then increases with the increase of parallel bond stiffness ratio $\overline{k}_n/\overline{k}_s$. The reason is that the difference between normal stiffness and tangential stiffness is increasing, that is, the increase of difference decreases the stability and strength of the specimen. Therefore, the internal friction angle is reduced appropriately, but not the cohesion. The internal friction angle increases with the parallel bond stiffness ratio. The reason is that the increase of the stiffness ratio of the parallel bond causes the rigid contact between particles. Furthermore, the overall "rigidity" of the experimental model increases, and its macrodamage gradually becomes tensile failure. $c_{max} = 9.29$ MPa is reached when the cohesion c of the direct shear test model is at the parallel bond stiffness ratio of $\overline{k}_n/\overline{k}_s = 1.45$. When $\overline{k}_n/\overline{k}_s < 1.45$, the cohesion of the specimen increases and then decreases with $\overline{k}_n/\overline{k}_s$.

The influence of parallel bond stiffness on internal friction angle is analyzed, as shown in Figure 3. In the conventional triaxial compression test, the internal friction angle increases with the ratio of parallel bond stiffness. In the direct shear test, the internal friction angle decreases with the increase of parallel bond stiffness ratio between particles, and its variation range is approximately 21%. $\overline{k}_n/\overline{k}_s = 6$, the internal friction angle of the conventional triaxial compression simulating test is $\varphi = 29.22^\circ$, and internal friction angle in the direct shear test is $\varphi = 18.83^\circ$. When $\overline{k}_n/\overline{k}_s > 3$, the internal friction angle of the specimen decreases gradually in the direct shear test. The influence of parallel bond stiffness on cohesion is analyzed, as shown in Figure 4. In the same parallel bond stiffness ratio, the cohesion obtained by the direct shear test is less than that of the conventional triaxial test but with a slight difference. The change trend of cohesion in the specimen is similar in both test conditions, that is, cohesion increases with $\overline{k}_n/\overline{k}_s$

Table 3: Shear strength parameter values under different particle contact moduli.

Particle contact modulus (GPa)	Friction angle (°)	Cohesion (MPa)
1	19.80	8.33
1.5	26.10	8.37
2	25.17	7.66
2.5	24.23	9.01
2.8	20.30	9.29
3.5	27.02	8.67
4	27.92	7.50
4.5	29.25	8.04
5	30.54	8.06
6	24.7	9.24
7	30.11	8.56

and reaches maximum and then decreases gradually at $\overline{k}_n/\overline{k}_s = 2$.

3.3. Particle Contact Modulus (EC). EC is the Young's modulus between particles, and the shear strength parameter values under different particle contact moduli are recorded, as shown in Table 3. In the direct shear test, internal friction angle and cohesion change due to the change of EC and the large variation amplitude. The internal friction angle is increasing gradually. When EC = 2.8 GPa, the internal friction angle of the specimens suddenly decreased to $\varphi = 20.30^\circ$, and cohesion reached the maximum value of $c = 9.29$ MPa. Although the internal friction angle decreases, the increased cohesion can enhance the shear strength of the structural plane. When the particle contact modulus is small, which is $1 \le E_C \le 2.8$ GPa, the change internal friction angle is significant, with a difference of 6.3°. The particle contact modulus, which strongly influences the internal friction angle, is relatively small. In actual simulation, EC should be adjusted constantly to match the actual internal friction angle. If EC is large, then the internal friction angle changes with it. The influence of EC on cohesion c is relatively small, with a difference of 1.79 MPa between the maximum cohesion and the minimum bond force, and the difference is approximately 19%. The friction angle of the maximum and minimum values is 10.74°, with a difference of approximately 35%.

The influence of EC on friction angle is shown in Figure 5. The internal friction angle obtained by the direct shear test is larger than that obtained by the triaxial compression test. With the increase of EC, the internal friction angle of the two experiments shows an increasing trend. The variation of internal friction angle in the direct shear test is large, whereas that in the triaxial compression test is stable. The influence of EC on cohesion is analyzed, as shown in Figure 6. Under the condition of two types of tests, the change trend of cohesion c is similar, but the cohesion obtained from the triaxial compression test is greater than that obtained from the direct shear test. The law is opposite from the internal friction angle changing law.

3.4. Parallel Bond Elastic Modulus. The elastic modulus $\overline{E}_c$ of the parallel bond is the Young's modulus of the bond between two particles. In the direct shear test, shear strength

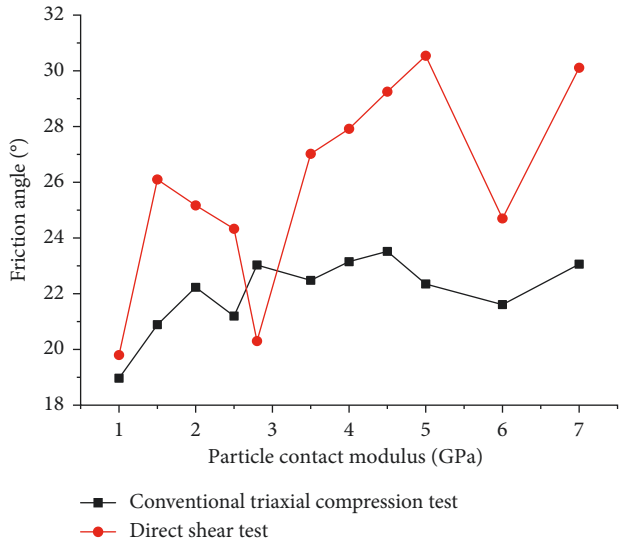

Figure 5: Influence of particle contact modulus on friction angle.

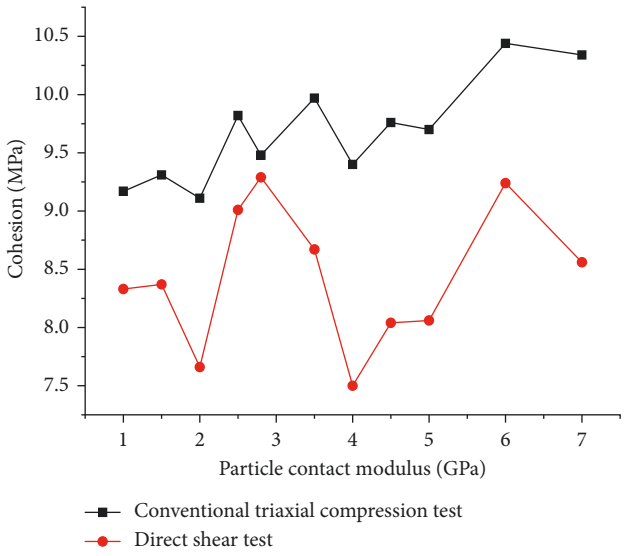

Figure 6: Influence of particle contact modulus on cohesion.

parameters φ and cohesion decrease with the increase of the parallel bond elastic modulus, as shown in Table 4. Parallel bond elastic modulus has a stronger impact on friction angle φ than that on cohesion c. The scope of the change of the internal friction angle is 5.44° or approximately 22%. The variation range of cohesion is 1.11 MPa or approximately 11%. Considering that friction angle and cohesion have a similar change trend with the parallel elastic modulus, the rule of Coulomb criterion [32–35] shows that larger parallel bond modulus means smaller internal friction angle and cohesion and shear strength. This phenomenon is due to the increase in the parallel bond elastic modulus, in which the mechanical properties of the specimens are changed, "rigidity" is enhanced, and shear strength is weakened.

The influence of the parallel bond elastic modulus on the internal friction angle is analyzed, as shown in Figure 7. In the triaxial compression and direct shear tests, the effect of

Table 4: Shear strength parameters of different parallel bond elastic moduli.

Parallel bond elastic modulus (GPa)	Friction angle (°)	Cohesion (MPa)
1	24.84	9.71
1.5	22.20	9.56
2	20.66	9.51
2.5	21.90	9.10
2.8	20.30	9.29
3.5	20.46	9.04
4	20.46	8.89
4.5	19.54	8.87
5	18.42	8.92
6	19.40	8.63
7	19.44	8.60

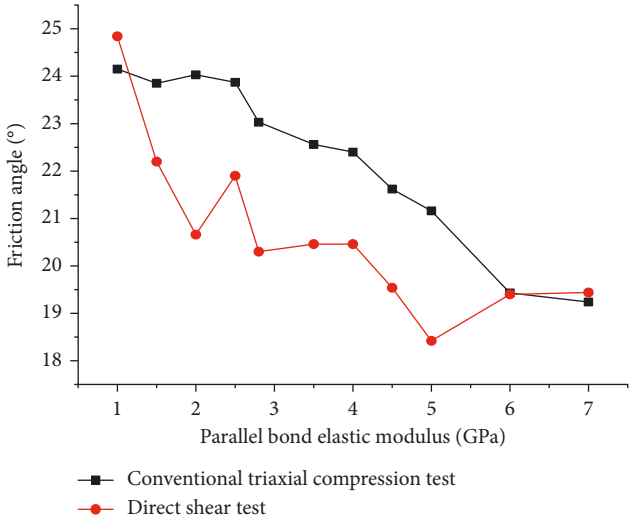

Figure 7: The effect of parallel bond elastic modulus on friction angle.

the elastic modulus ($\overline{E}_c$) of the parallel bond on the internal friction angle is much the same. The internal friction angle decreases and the internal friction angle of the triaxial compression test is larger than that of the straight shear test with the increase of the elastic modulus $\overline{E}_c$ of the parallel bond. When the parallel bond elastic modulus is equal to 6 GPa, the internal friction angle obtained in the two experiments is approximately equal. The difference in the internal friction angle is small under the condition of two kinds of test along with the increase of $\overline{E}_c$ when $\overline{E}_c = 7$ GPa. A large parallel-bonded elastic modulus can be achieved by using the internal friction angle from the conventional triaxial compression test as the actual internal friction angle. Figure 8 shows the effect of the parallel bond elastic modulus on cohesion. The variations of cohesion and internal friction angle and the influence trend of the adhesive modulus are roughly the same. In addition, the cohesion obtained under the two test conditions is approximately the same. Only when $\overline{E}_c < 2$, the difference between the two conditions is large and the cohesion obtained by the triaxial compression test is larger than that obtained by the direct shear test.

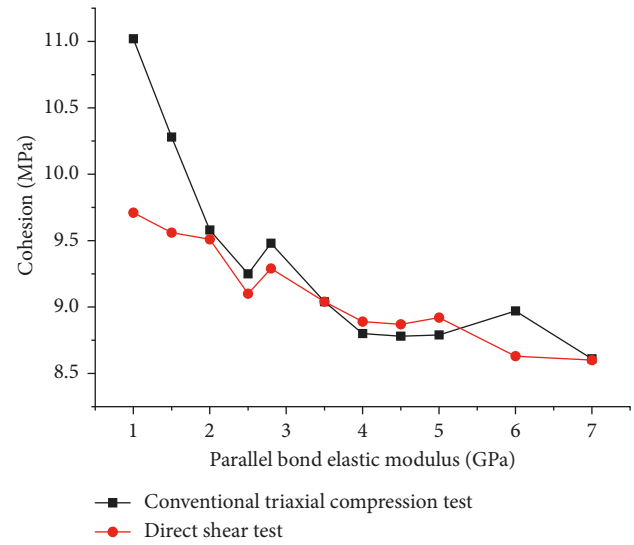

Figure 8: Influence of parallel bond elastic modulus on cohesion.

Table 5: Shear strength of different particle size specimens under normal stress.

Minimum particle size (mm)	Normal stress (MPa)					
	2.5	5	7.5	10	12.5	15
0.20	8.64	10.64	12.02	13.04	13.28	14.19
0.25	8.21	11.08	12.01	12.42	13.60	14.51
0.28	9.82	11.25	12.62	12.85	13.96	14.60
0.4	10.00	11.57	12.34	12.48	12.85	14.48
0.5	9.71	10.93	12.20	12.73	13.32	14.28
0.8	10.86	12.39	14.03	15.16	15.67	16.41
1.0	10.81	11.68	12.88	13.90	14.72	15.33
1.2	10.97	12.46	13.04	13.59	13.81	14.88
1.5	11.43	13.06	13.77	15.17	15.40	16.35

3.5. Particle Size. According to the numerical simulation test and studies by other scholars, the size of a particle significantly influences the shear strength of the specimen [1]. Therefore, the influence of particle size on shear strength parameters is discussed. The minimum particle size is set to 0.20, 0.25, 0.28, 0.4, 0.5, 0.8, 1.0, 1.2, and 1.5 mm. The particle diameter ratio of the specimen was set to 1.5, and the shear strength of the specimens with different particle sizes was obtained under normal stress by controlling the particle size ratio, as shown in Table 5. Under the same normal stress conditions, the shear strength of the specimens increases with particle size. When the particle size was more than 0.8 mm, the particle size has less influence on shear strength. The effect of particle size on shear strength decreases with the increase of normal stress. When the minimum particle size is 0.8 mm and 1.5 mm, the shear strength is closer to the increase of the normal stress.

Table 6 shows that in the direct shear test, the influence of the particle size of a specimen on the friction angle φ is greater than cohesion c. Cohesion increases with the particle size, and the range is 2.86 MPa or approximately 26%. The effect of the particle size of a specimen on internal friction angle is large, the range is 8.85° or approximately 36%, and

Table 6: Shear strength parameter values of different particle sizes.

Minimum particle size (mm)	Friction angle (°)	Cohesion (MPa)
0.2	22.73	8.30
0.25	24.28	8.03
0.28	20.30	9.29
0.4	16.75	9.64
0.5	19.24	9.14
0.8	23.89	10.21
1.0	20.51	9.95
1.2	15.43	10.71
1.5	20.66	10.89

Table 7: Shear strength of specimens with different particle size ratios under normal stress.

Particle size ratio	Normal stress (MPa)					
	2.5	5	7.5	10	12.5	15
1.5	9.82	11.25	12.62	12.85	13.96	14.60
2.0	9.72	11.27	12.73	13.62	14.02	15.45
2.5	9.20	10.65	12.00	12.60	13.19	13.78
3.0	8.57	10.59	11.28	11.88	12.64	13.76

the internal friction angle decreases without obvious regularity. For a minimum particle size of 0.25 mm and 1.2 mm, the internal friction angle reaches its maximum and minimum values of $\varphi_{max} = 24.28^{\circ}$ and $\varphi_{min} = 15.43^{\circ}$, respectively.

3.6. Particle Size Ratio. The particle size ratio is the ratio of the maximum particle size to the minimum particle size. Controlling the minimum particle size (0.28 mm), changing the particle size ratio of 1.5, 2.0, 2.5, and 3.0, and obtaining the shear strength of the specimens with different particle size ratios under normal stress are shown in Table 7. The direct shear test is conducted when the normal stress is 2.5 MPa, and the shear strength of the specimen gradually decreases with the increase of the particle size ratio. When the normal stress exceeds 2.5 MPa, the shear strength of the specimen reaches the maximum when the particle size ratio is 2.0. Thereafter, the shear strength decreases with the increase of particle size ratio. The direct shear test is conducted on a certain particle size ratio, and the shear strength of the specimen increases continuously with the increase of normal stress. In summary, although the increase of the particle size ratio increases the instability of the specimen, the shear strength of the particle size is highest when the particle size ratio is 2.0.

The shear strength parameter values of different particle size ratios (Table 8) show that in the direct shear test, the impact of particle size ratio on the cohesion of the specimen is relatively small. Cohesion decreases with the increase of the particle size ratio, and the decrease range is 1.11 MPa or approximately 12%, indicating that the increase of particle size ratio decreases the overall mechanical property of the specimen. Shear strength is the largest when the particle size ratio is 2.0 because of the increase in shear strength due to the increase of the friction angle when the cohesion decreases. The overall shear performance of the specimen decreases with the increase of the particle size ratio mainly due to the decrease of cohesion.

Table 8: Shear strength parameter values of different particle size ratios.

Particle size ratio	Friction angle (°)	Cohesion (MPa)
1.5	20.30	9.29
2.0	23.36	9.03
2.5	19.60	8.79
3.0	20.51	8.18

4. Conclusions

(1) The internal friction angle φ of the structural plane decreases with the increase of particle contact stiffness ratio. The internal friction angle decreases first and then increases with the increase of parallel bond stiffness ratio.

(2) In the same parallel bond stiffness ratio $\overline{k}_n/\overline{k}_s$, the cohesion obtained by the direct shear test is less than that of the conventional triaxial test but with a slight difference. Cohesion increases with $\overline{k}_n/\overline{k}_s$ and reaches maximum and then decreases gradually at $\overline{k}_n/\overline{k}_s = 2$.

(3) The influence of particle contact modulus EC on cohesion c is relatively small. The internal friction angle obtained by the direct shear test is larger than that obtained by the triaxial compression test. With the increase of EC, the internal friction angle shows an increasing trend.

(4) The shear strength of the specimens increases with particle size. Cohesion increases with the particle size. The shear strength of the specimen gradually decreases with the increase of the particle size ratio. The impact of particle size ratio on the cohesion of the specimen is relatively small.

Data Availability

The data used to support the findings of this study are available from the corresponding author upon request.

Conflicts of Interest

The authors declare no conflicts of interest.

References

[1] M. Bahaaddini, P. C. Hagan, R. Mitra, and B. K. Hebblewhite, "Parametric study of smooth joint parameters on the shear behaviour of rock joints," *Rock Mechanics and Rock Engineering*, vol. 48, no. 3, pp. 923–940, 2015.

[2] N. Barton, "Review of a new shear-strength criterion for rock joints," *Engineering Geology*, vol. 7, no. 4, pp. 287–332, 1973.

[3] R. Cao, P. Cao, H. Lin, and X. Fan, "Experimental and numerical study of the failure process and energy mechanisms of rock-like materials containing cross un-persistent joints

under uniaxial compression," *PLoS One*, vol. 12, no. 12, Article ID e0188646, 2017.

[4] W. G. Pariseau, S. Puri, and S. C. Schmelter, "A new model for effects of impersistent joint sets on rock slope stability," *International Journal of Rock Mechanics and Mining Sciences*, vol. 45, no. 2, pp. 122–131, 2008.

[5] M. Jiang, T. Jiang, G. B. Crosta, Z. Shi, H. Chen, and N. Zhang, "Modeling failure of jointed rock slope with two main joint sets using a novel DEM bond contact model," *Engineering Geology*, vol. 193, pp. 79–96, 2015.

[6] H. Lin, Z. Xiong, T. Liu, R. Cao, and P. Cao, "Numerical simulations of the effect of bolt inclination on the shear strength of rock joints," *International Journal of Rock Mechanics and Mining Sciences*, vol. 66, pp. 49–56, 2014.

[7] A. Ghazvinian, V. Sarfarazi, W. Schubert, and M. Blumel, "A study of the failure mechanism of planar non-persistent open joints using PFC2D," *Rock Mechanics and Rock Engineering*, vol. 45, no. 3, pp. 677–693, 2012.

[8] G. Grasselli, "3D behaviour of bolted rock joints: experimental and numerical study," *International Journal of Rock Mechanics and Mining Sciences*, vol. 42, no. 1, pp. 13–24, 2005.

[9] Y. Gui, C. C. Xia, W. Q. Ding, X. Qian, and S. G. Du, "A new method for 3D modeling of joint surface degradation and void space evolution under normal and shear loads," *Rock Mechanics and Rock Engineering*, vol. 50, no. 10, pp. 2827–2836, 2017.

[10] M. S. Asadi, V. Rasouli, and G. Barla, "A bonded particle model simulation of shear strength and asperity degradation for rough rock fractures," *Rock Mechanics and Rock Engineering*, vol. 45, no. 5, pp. 649–675, 2012.

[11] M. S. Asadi, V. Rasouli, and G. Barla, "A laboratory shear cell used for simulation of shear strength and asperity degradation of rough rock fractures," *Rock Mechanics and Rock Engineering*, vol. 46, no. 4, pp. 683–699, 2013.

[12] S. Q. Yang and Y. H. Huang, "Particle flow study on strength and meso-mechanism of Brazilian splitting test for jointed rock mass," *Acta Mechanica Sinica*, vol. 30, no. 4, pp. 547–558, 2014.

[13] J. Yang, G. Rong, D. Hou, J. Peng, and C. B. Zhou, "Experimental study on peak shear strength criterion for rock joints," *Rock Mechanics and Rock Engineering*, vol. 49, no. 3, pp. 821–835, 2016.

[14] N. Fardin, O. Stephansson, and L. R. Jing, "The scale dependence of rock joint surface roughness," *International Journal of Rock Mechanics and Mining Sciences*, vol. 38, no. 5, pp. 659–669, 2001.

[15] J. W. Park and J. J. Song, "Numerical simulation of a direct shear test on a rock joint using a bonded-particle model," *International Journal of Rock Mechanics and Mining Sciences*, vol. 46, no. 8, pp. 1315–1328, 2009.

[16] P. S. Andrade and A. A. Saraiva, "Estimating the joint roughness coefficient of discontinuities found in metamorphic rocks," *Bulletin of Engineering Geology and the Environment*, vol. 67, pp. 425–434, 2008.

[17] N. Fardin, Q. Feng, and O. Stephansson, "Application of a new in situ 3D laser scanner to study the scale effect on the rock joint surface roughness," *International Journal of Rock Mechanics and Mining Sciences*, vol. 41, no. 2, pp. 329–335, 2004.

[18] Z. Y. Yang, C. C. Di, and S. C. Lo, "Two-dimensional hurst index of joint surfaces," *Rock Mechanics and Rock Engineering*, vol. 34, no. 4, pp. 323–345, 2001.

[19] J. Yoon, "Application of experimental design and optimization to PFC model calibration in uniaxial compression simulation," *International Journal of Rock Mechanics and Mining Sciences*, vol. 44, no. 6, pp. 871–889, 2007.

[20] J. Jin, P. Cao, Y. Chen, C. Pu, D. Mao, and X. Fan, "Influence of single flaw on the failure process and energy mechanics of rock-like material," *Computers and Geotechnics*, vol. 86, pp. 150–162, 2017.

[21] M. H. Mehranpour and P. H. S. W. Kulatilake, "Improvements for the smooth joint contact model of the particle flow code and its applications," *Computers and Geotechnics*, vol. 87, pp. 163–177, 2017.

[22] W. L. Tian and S. Q. Yang, "Experimental and numerical study on the fracture coalescence behavior of rock-like materials containing two non-coplanar filled fissures under uniaxial compression," *Geomechanics and Engineering*, vol. 12, no. 3, pp. 541–560, 2017.

[23] X. Fan, P. H. S. W. Kulatilake, X. Chen, and P. Cao, "Crack initiation stress and strain of jointed rock containing multi-cracks under uniaxial compressive loading: a particle flow code approach," *Journal of Central South University*, vol. 22, no. 2, pp. 638–645, 2015.

[24] D. He and Y. Cheng, "Numerical simulation for mechanical behavior of asphalt pavement with graded aggregate base," *Advances in Civil Engineering*, vol. 2018, Article ID 1404731, 9 pages, 2018.

[25] R. Cao, W. Tang, H. Lin, and X. Fan, "Numerical analysis for the progressive failure of binary-medium interface under shearing," *Advances in Civil Engineering*, vol. 2018, Article ID 4197172, 11 pages, 2018.

[26] K. Farahmand, I. Vazaios, M. S. Diederichs, and N. Vlachopoulos, "Investigating the scale-dependency of the geometrical and mechanical properties of a moderately jointed rock using a synthetic rock mass (SRM) approach," *Computers and Geotechnics*, vol. 95, pp. 162–179, 2018.

[27] J. Shang, Z. Zhao, and S. Ma, "On the shear failure of incipient rock discontinuities under CNL and CNS boundary conditions: insights from DEM modelling," *Engineering Geology*, vol. 234, pp. 153–166, 2018.

[28] T. Kazerani, Z. Y. Yang, and J. Zhao, "A discrete element model for predicting shear strength and degradation of rock joint by using compressive and tensile test data," *Rock Mechanics and Rock Engineering*, vol. 45, no. 5, pp. 695–709, 2012.

[29] P. H. S. W. Kulatilake, G. Shou, T. H. Huang, and R. M. Morgan, "New peak shear strength criteria for anisotropic rock joints," *International Journal of Rock Mechanics and Mining Sciences and Geomechanics Abstracts*, vol. 32, no. 7, pp. 673–697, 1995.

[30] S. Xu and M. H. D. Freitas, "Use of a rotary shear box for testing the shear strength of rock joints," *Geotechnique*, vol. 38, no. 2, pp. 301–309, 1988.

[31] X. Zhang, Q. Jiang, N. Chen, W. Wei, and X. Feng, "Laboratory investigation on shear behavior of rock joints and a new peak shear strength criterion," *Rock Mechanics and Rock Engineering*, vol. 49, no. 9, pp. 1–18, 2016.

[32] Y. Zhao, J. Tang, Y. Chen et al., "Hydromechanical coupling tests for mechanical and permeability characteristics of fractured limestone in complete stress-strain process," *Environmental Earth Sciences*, vol. 76, no. 1, p. 24, 2017.

[33] H. Lin, W. Xiong, and Q. Yan, "Three-dimensional effect of tensile strength in the standard brazilian test considering contact length," *Geotechnical Testing Journal*, vol. 39, no. 1, pp. 137–143, 2016.

[34] H. P. Yuan, P. Cao, and W. Z. Xu, "Mechanism study on subcritical crack growth of flabby and intricate ore rock," *Transactions of Nonferrous Metals Society of China*, vol. 16, no. 3, pp. 723–727, 2006.

[35] X. Fan, P. H. S. W. Kulatilake, and X. Chen, "Mechanical behavior of rock-like jointed blocks with multi-non-persistent joints under uniaxial loading: a particle mechanics approach," *Engineering Geology*, vol. 190, pp. 17–32, 2015.